Proposed Methodology for Routine Asteroid Spectroscopy

Arthur C. Lucas
and
David Lien

Oklahoma State University

Presented
at
MPAPW
Minor Planet Amateur/Professional Workshop

Phoenix, AZ
June 13, 2003

Proposed Methodology for Routine Asteroid Spectroscopy

Arthur C. Lucas and David Lien

1.0 Introduction. Light reflected from asteroids is often typified by the photography of the asteroid through a series of optical filters and, then, categorizing its color by specifying a series of color indices such as UBV or UVBRI. The color indices may also be created by integrating selectively over regions of an optical spectrum. In this application a high resolution spectrum is not required as would be the case if one were looking for resident chemistry in the object. A convergent beam, grating spectrometer provides satisfactory resolution and simple operation in this application.

While the spectrometer is simple to operate, a goal of amateur, minor planet observers is operation over the widest possible range of magnitudes in the observed object. The work reported here has been developed with an eye to optimizing dispersion, focussing, data reduction, and aberration correction so as to maximize the magnitude range for the system as it applies to operation with a CCD camera.

2.0 Initial Performance Evaluation. A quick and easy implementation of the system was had by installing a Rainbow Optics grating into a position on the filter wheel of the SBIG CFW-8 filter changer. The filter changer was mounted on the SBIG ST-8 camera. The camera was mounted to a Celestron C8, 8-inch telescope. An f 3.3 compressor lens was added to the output of the telescope to provide a wider view of the sky..

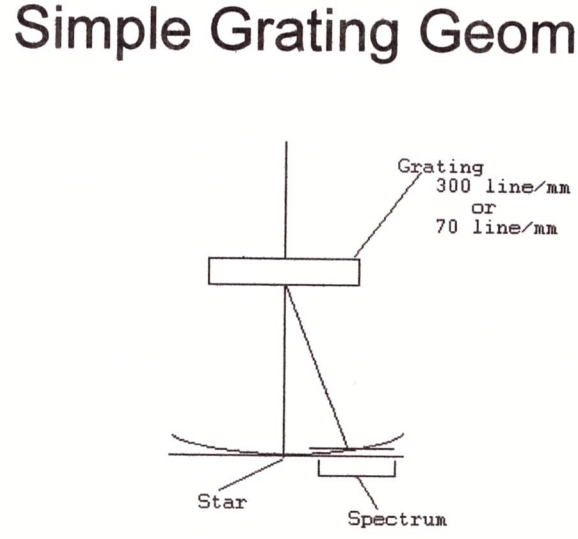

Figure 1. Sketch of the grating geometry. The grating is placed close to the focal plane of the CCD camera.

2.1. Stellar Images. Figure 2 shows a typical photograph of a star field. In this case it is the open cluster, M44.

Figure 2. Typical view of a star field, M44, photographed with the grating in place.

Just above the center of the photo are two stars. The lower, left star is SAO 80336 at mag 6.61 classed as Spectral type A1V. To its right and a little up is SAO80333 at mag 6.39 classed as Spectral type K0III. The streaks which follow from the stars to the lower right represent the diffracted light in which the spectral information resides. The spectrum may be derived by measuring the peak brightness in the diffracted line starting from the coordinates of the star.

Calculational Model

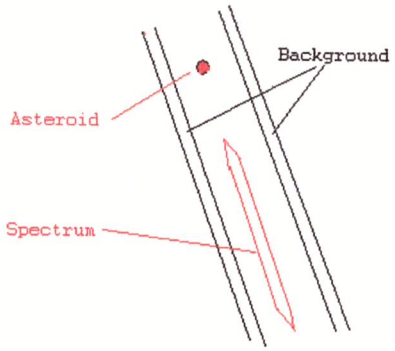

Figure 3. Sketch of the calculational model.

. Figure 3 shows a sketch of the calculational model. The model acquires horizontal image lines one-by-one. The computation looks for the peak brightness in the central trace. Background regions are established to the right and left of the central trace. While the backgrounds may be adjusted in the model, much of the work which follows used a 10 pixel wide strip, set 10 to 20 pixels from the central ray for the background.

```
OPEN "c:\starspex\" + ns$ + ".st8" FOR BINARY AS #1
      sc = 2048                  'front matter
FOR y = 1 TO 1000                'image data lines
            wide = 3060
   FOR x = 1 TO wide               'get all the bytes
                                   'first 2 are the number in a line
         SEEK #1, x + sc           'next 2 are fixed lo, hi format
       d1(x) = ASC(INPUT$(1, #1))
   NEXT x
      sc = sc + wide
      j = 0
FOR i = 1 TO wide STEP 2                'calculate pixels
         j = j + 1
    dta(j) = d1(i) + 256 * d1(i + 1)
 NEXT i
NEXT y
```

Figure 4. Primary code for reading the non-compressed image. The code is written in Microsoft QUICKBASIC version 4.5.

The image is saved in SBIG non-compressed format. Note that the conventional storage is in compressed format. The primary code for reading the data is shown in Figure 4. The code is written in Microsoft QUICKBASIC version 4.5. The remainder of the fairly extensive coding follows simple principles of computation. Once the background corrected brightness along the central ray is determined and saved in an array any required computation may be performed.

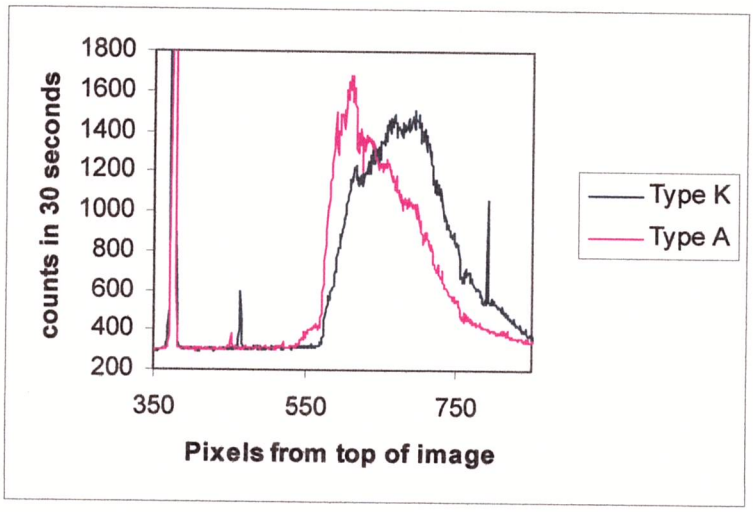

Figure 5. Original data obtained by finding the peak brightness along a line extending from the star and along the path of diffraction. Note that the position of the star is always the location of zero wavelength.

Figure 5 shows a graph of those data for the two stars referenced above. The location of the star represents the location of zero in the diffracted image and is a valuable reference. Several sharp peaks are present in the pattern which are attributable to stars along the path of the diffraction line. This represents one of the issues in careful application of the method. Either the software used to find the diffracted line must be able to discriminate against them or visual review of the image must be employed in order that these lines not be attributed to discrete emission lines.

A part of any program to employ this method must involve calibration in both wavelength as a function of pixel distance and sensitivity of the detector as a function of wavelength. As these values have not been established independently for the moment, wavelength calibration is estimated from the position of the absorption line at 383 pixels. This line is believed to represent absorption due to the Hα resonance at 656 nm. Taking that to be the wavelength calibration, the graph of Figure 6 is plotted in terms of wavelength.

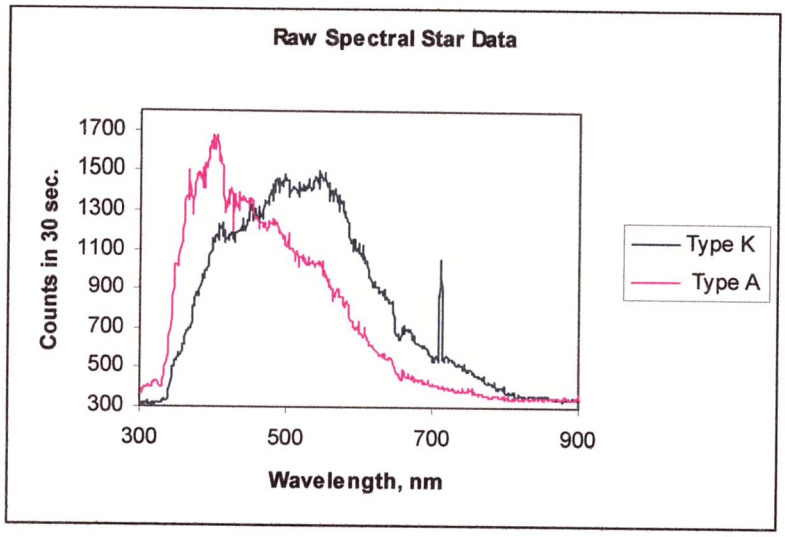

Figure 6. Spectrum of stars SAO 80336 and SAO 80333 shown above. The spectrum is derived by measuring the maximum brightness along the diffracted line. The sharp peak at about 700 nm is the brightness of an interfering star and not a spectral line. The calibration is estimated by the position of the Hα absorption.

Further validation of the method in identifying widely varying characteristics of stars is obtained by observing the spectra of Betelgeuse and Regulus.

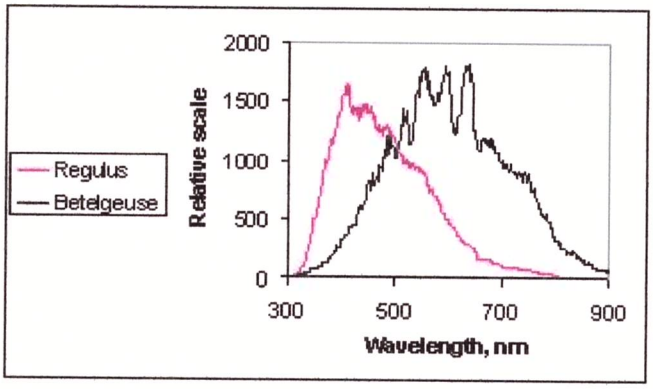

Figure 7. Spectrum of Betelgeuse, a Type M21b star along with Regulus, a B7V star.

The image shows the very red star spectrum contrasted with the nearly blue light of Regulus. These images are presented to characterize the system at the beginning of the project and to form a foundation for observing asteroids.

2.2. Asteroid Images. Asteroid images are apt to resemble the solar spectrum with

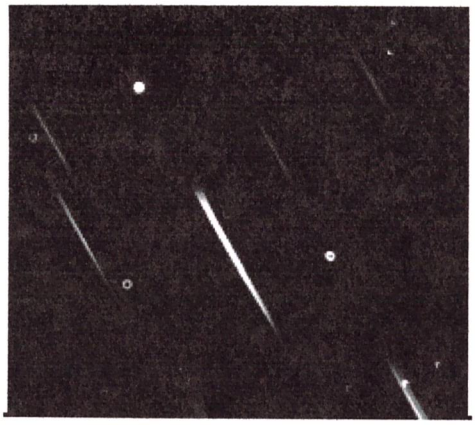

Figure 8. Image of asteroid 4 Vesta. The primary image is deliberately out of focus in order to focus on the diffracted image.

occasional absorption/reflection nuances. The principle objective in this work is to establish the ability to measure the diffracted light with sufficient accuracy to describe those absorption/reflection nuances. To that end we start with an image of Vesta, shown in Figure 8, at high enough brightness to observe the spectrum easily with some accuracy.

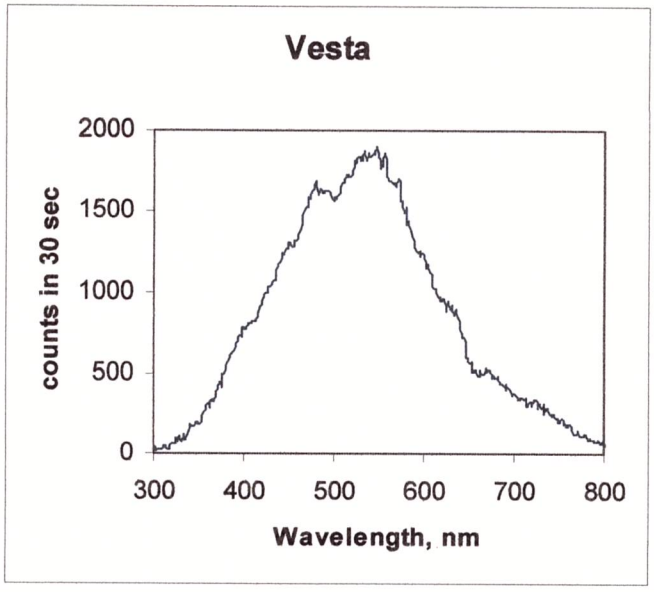

Figure 9. Spectrum of Vesta. The predicted magnitude was 6.17 at that time.

The derived spectrum, shown in Figure 8, shows some detail and mostly visible, yellow to red light.

A significant step down in brightness was taken in choosing 37 Fides as an asteroid of intermediate difficulty of recording. At the time of the image below it was at magnitude 10.73. Ten 60 second images were recorded in succession. An evaluation of the several

images permits a determination of the accuracy of measurement at this magnitude and with the instrumentation in place at the time of measurement.

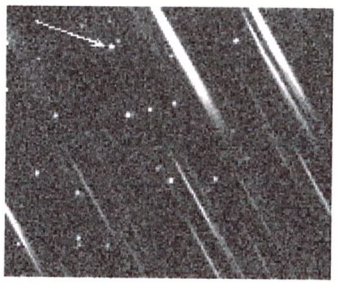

Figure 10. Photo of asteroid 37 Fides. The exposure time is 60 seconds. The predicted magnitude is 10.73 at the time of the photo.

One of the images is shown in Figure 10. The image was taken with the quarter moon 75 degrees away at the time.

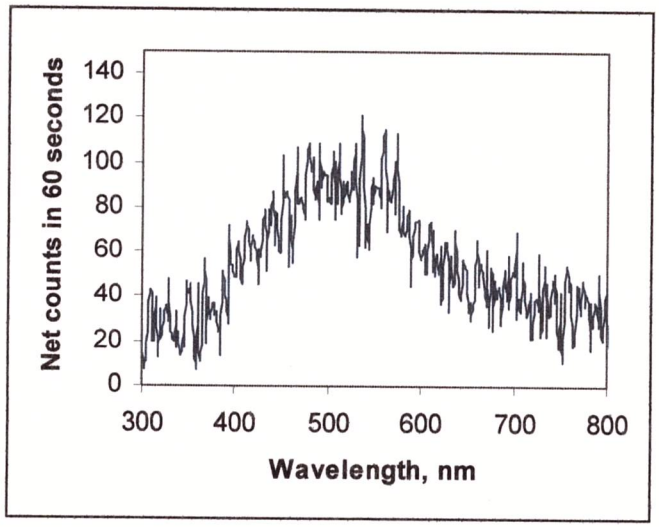

Figure 11. Spectrum of 37 Fides derived from a single 60 second exposure. The sky background for this exposure was 528 counts in a pixel...

The derived spectrum for the image shown above is shown in Figure 11. Care should be taken to note that the eventual goal of this work is to sum the spectrum in defined regions, resulting in statistical improvement in the final data. In order to begin the process of finding the credibility of the final number, the 10 spectra were derived for the 10 images. The average spectrum representing all 10 images is shown in Figure 12.

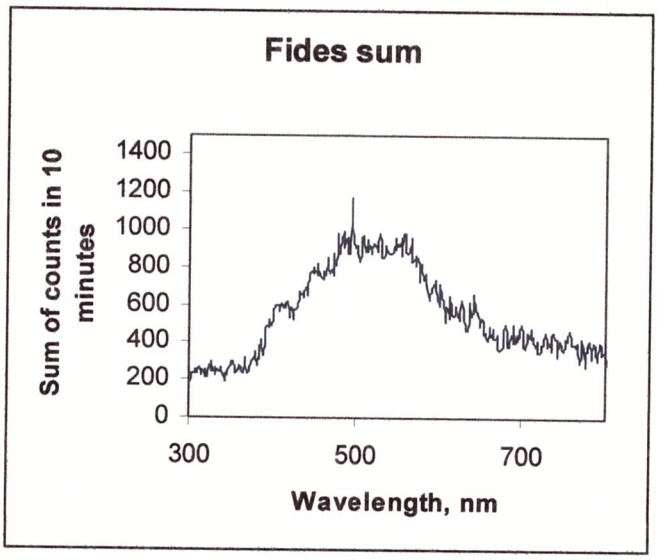

Figure 12. Spectrum of 37 Fides derived from the sum of 10 each 60 second images...

3.0 Prism Correction of Aberration. In accordance with the suggestions by Buil, a low angle prism has been inserted into the beam along with the grating. The idea is that the focussing will be sharper, resulting in brighter images and less interference between objects.

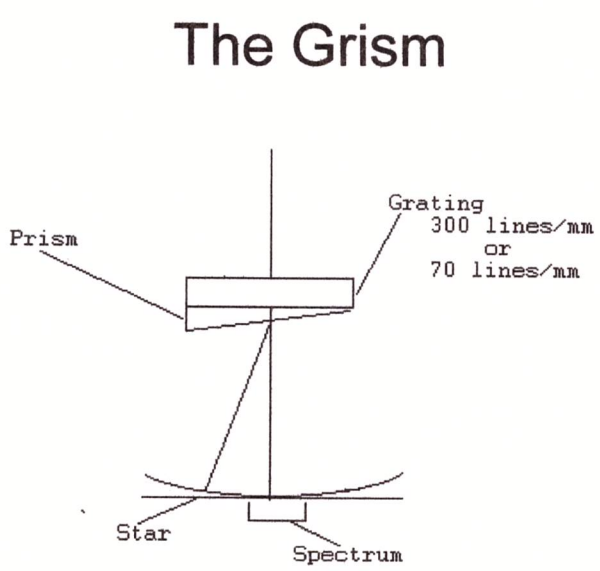

Figure 13. Sketch of the geometry of the GRISM as conceived by Buil.

The prism was placed in contact with the Rainbow prism. Only an air interface was used. That is to say, there was no optical coupling medium used in the assembly. A few images were accumulated to estimate the enhancement of focussing. An objective comparison is shown in Figure 14. The diffracted line is clearly somewhat sharper perhaps resulting in up to a factor of 2 in peak brightness.

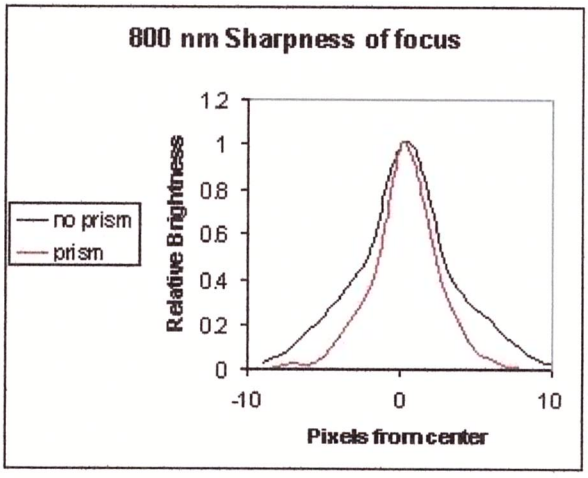

Figure 14. Comparison of point spread function with and without the correcting prism. The prism is used in conjunction with the 300 line/mm grating.

4.0 Coarse Grating Performance. The grating demonstrated above has 300 lines/mm. A 70 line/mm grating would compress the diffracted image by a factor of 3. This would yield an image of greater brightness and reduce interference between objects. Accordingly a 1-inch square, 70 line/mm grating was procured from Edmund Scientific. The grating was mounted approximately 12 mm from the SBIG ST-8 CCD detector to compress the diffracted images as much as possible. The mounting consisted of a brass plate with screw threads on its perimeter so as to allow its being placed at any one of several distances by using combinations of T-adaptors. The grating is lightly held in place with a small set screw set radially through the edge of the plate.

The first image of 37 Fides made with the 70 lines/mm grating is shown in Figure 15. The diffracted images are short. The -1 diffraction order is greatly suppressed. The +2 order is obvious but not objectionable. The image was created using an exposure time of 10 minutes with the Celestron C8, Meade f 3.3 Focal Reducer, and the SBIG St-8 camera.

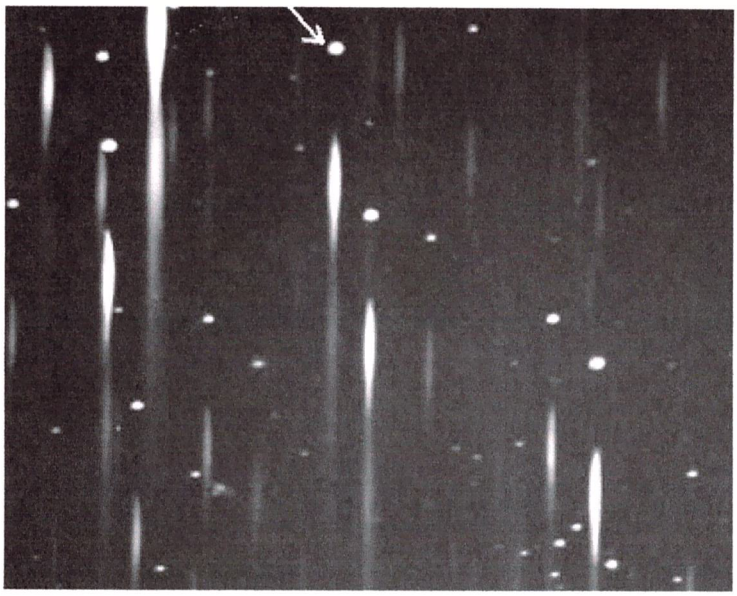

Figure 15. Image of 37 Fides made with the 70 line/mm grating in place at 12 mm from the focal plane. This is the first image of 37 Fides taken with the 70 mm grating. The exposure time was 10 minutes. The seeing was uniformly a little hazy. The low dispersion combined with a short, 12 mm, distance from the grating to the CCD array shorten the image with a consequential increase in brightness. Work that follows will be directed at optimizing the readout method so as to optimize signal to noise ratio. Following that, the greatest detectable magnitude(least brightness) will be determined as a function of exposure time.

The derived spectrum is shown in Figure 16. The counting rate has increased to a peak value of 3500 from a value of 700 in the first example shown in Figure 12 above. The data in the figure are derived by finding the peak value of all pixels to the left and right of the center of the estimated centerline.

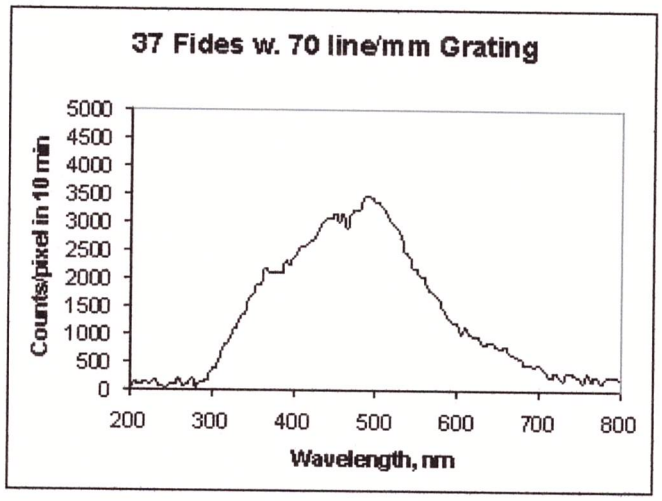

Figure 16. The spectrum of 37 Fides derived from the image of Figure 15.

Figure 16 shows the spectrum of 37 Fides derived from the image of Figure 15. The textbook magnitude of the asteroid at this time was 10.9. The exposure time was 10 minutes using the Celestron C8 with the SBIG ST-8. The 70 line/mm grating was approximately 12 mm from the CCD image plane. The values shown are single pixel values taken to be the maximum in a region +- 10 pixels from the path. In that simplistic mode the shape of the spectrum may be somewhat sensitive to focussing. We shall see below, however, that the shape remains essentially invariant with averaging over as many as 15 pixels. The shape also is closely matched to a nearby star, GSC 843.658. The most important improvement remaining in this development is to improve the optics so as to create smaller star images. Optimally this should be a reduction of a factor of two. Greater reduction in the point spread distribution would be lost in pixel size.

Some improvement might be had by averaging pixels. Accordingly, additional.spectra were derived for 3, 5, 7, 9, 11, 13, and 15 pixels. The detectability for faint objects was estimated by finding the variance on the part of the spectra between 200 and 300 nm. Figure 17 shows the results of that calculation. Some advantage in detectability can be had, in this case, by averaging to the left and right up to 7 pixels. A further test that

remains is to determine the extent to which focussing irregularities might require such averaging.

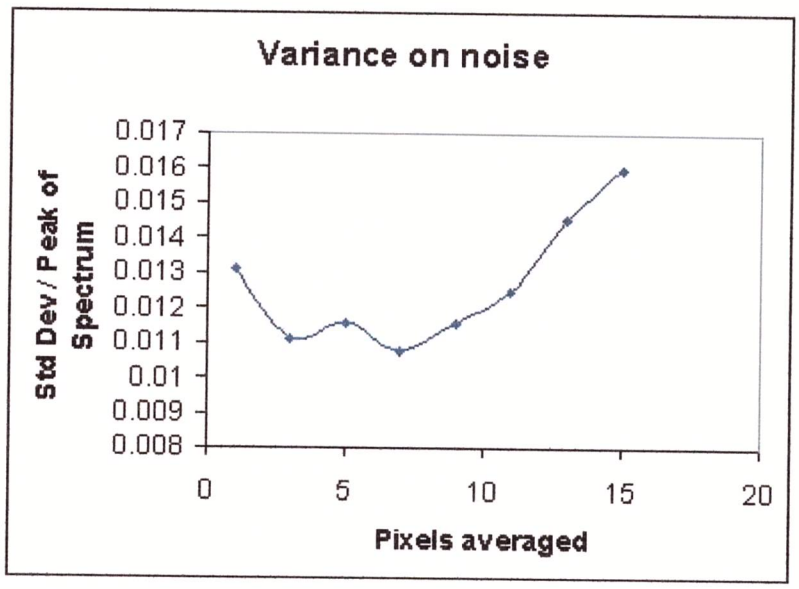

Figure 17. Variance on noise in the spectrum for a range of lateral averaging widths.

The randomness of the data are estimated by finding the standard deviation on the data in the region 200-300 nm. This graph shows the result of laterally averaging pixels across the identified peak in the diffracted image. Some improvement in randomness is found as more pixels are averaged. As the averaging continues, the value of the peak is diminished making the denominator in the variance calculation less. So the optimum FOR THIS PARTICULAR ARRANGEMENT is 3 to 7 pixels. No averaging was done in the wavelength direction.

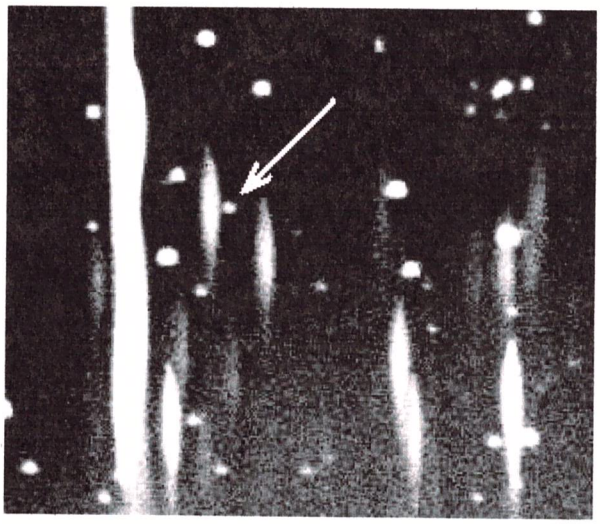

Figure 18. Image of mag 14.27 asteroid 90 Antiope using the 70 line/mm grating and a 10 minute exposure.

Figure 18 shows a cropped SBIG ST-8 image of 14.3 magnitude Antiope. The diffracted image is visible below the marked primary image. The image was formed using a Celestron C8 telescope with an f3.3 Focal Reducer, a 70 line/mm grating and an exposure time of 10 minutes.

The image is presented as an example of limiting detectability of the diffracted light signal.

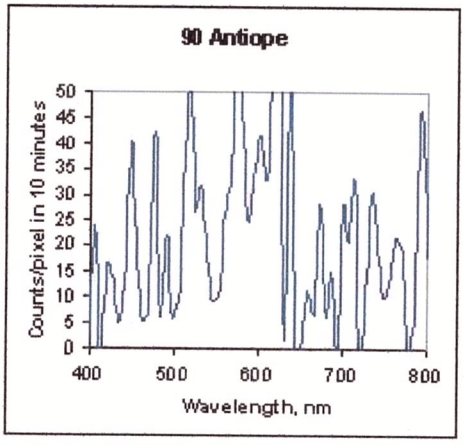

Figure 19. Spectrum derived from the image of Fig. 18. The spectrum is quite noisy as a result of the background noise in the image.

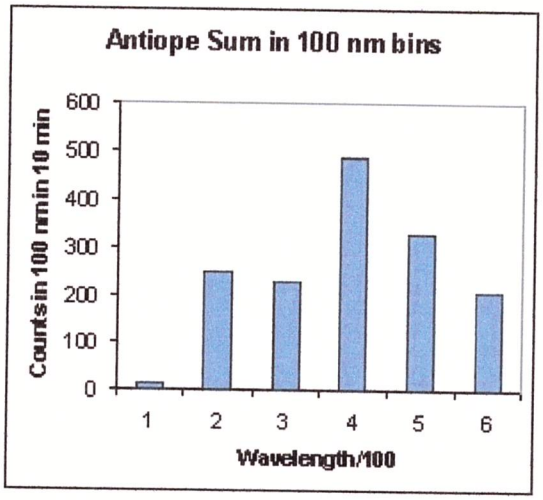

Figure 20. Bar graph illustrating the use of the noisy data of Fig. 19 in forming the integrated functions UBVRI. In this case the data are integrated over even intervals of 100 nm. The bars at 200 and 300 nm are over estimated due to an interfering star.

Improvement in the detectability can be had only by (a) integrating the image over a longer time, (b) focus the image more sharply using lenses (c) Use a larger telescope to collect more light. These issues will be pursued as this work develops.

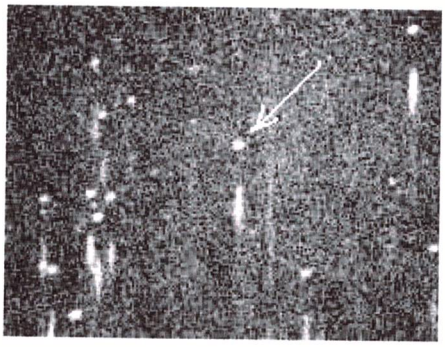

Figure 21. Image of 921 Jovita at magnitude 14.4.

A major improvement in signal/noise ratio was obtained by removing the f 3.3 focal reducer. This has the effect of making the distributed background in the image darker. The first image obtained in this way is shown in Figure 21. The derived spectrum is shown in Figure 22. As the ultimate goal of this work is to sum the spectrum over the response of the UBVRI filter functions, an example of the effect of such smoothing over a nominal band 100 nm wide is shown in Figure 23.

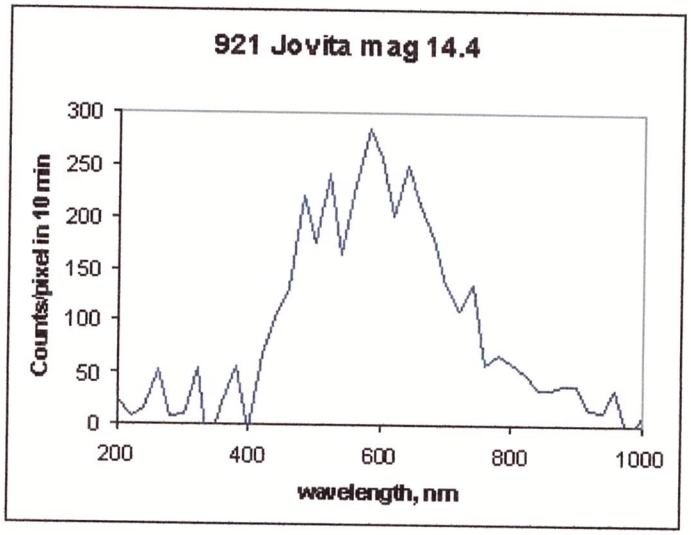

Figure 22. Spectrum of 921 Jovita derived from the image of Figure 21.

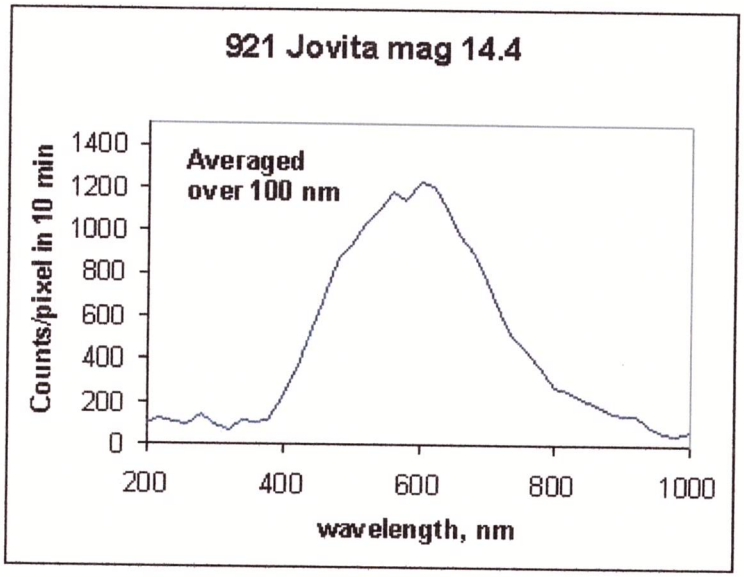

Figure 23. Spectrum of 921 Jovita smoothed over 100 nm bin widths.

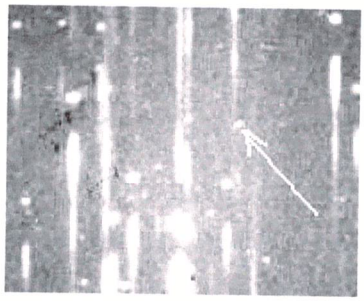

Figure 24. Image of 938 Chlosinde at magnitude 15.9

The ultimate detectability of the system is shown in Figure 24. This image was created using the CCDSOFT feature which takes sequential images which may then be placed into accurate registration and summed. In this case, 30 each, 30 second images were accumulated. The summed image shows the asteroid moving toward the northwest during the duration of the sequence.

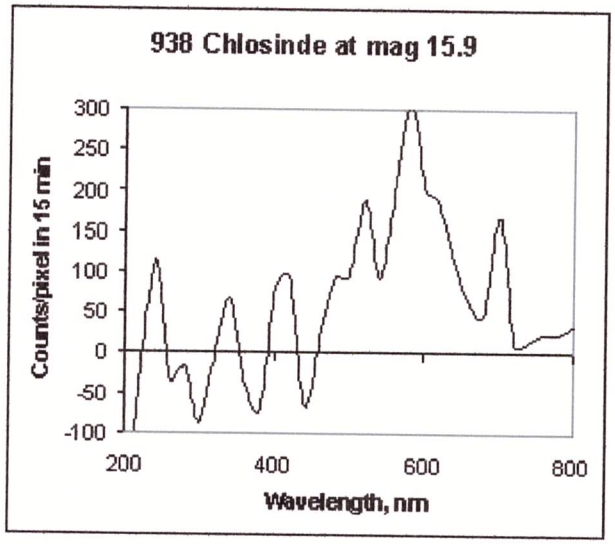

Figure 25. Spectrum of the asteroid 938 Chlosinde at magnitude 15.9 derived from the image of Figure 24.

The spectrum, shown in Figure 25, while noisy, indicates that magnitude 16 spectroscopy with the apparatus described above is difficult, but possible. Subsequent work using self guiding indicates significant improvement over the image of figure 24. Satisfactory spectroscopy for such faint objects is projected to require one hour of imaging. The best way to accomplish this is to take a series of self guided images each 10 minutes long and co-add them.

5.0. Wavelength Dependence of the CCD. None of the spectra shown above have been either reduced to absolute values of energy flux or corrected for the wavelength

dependence of the silicon CCD chip. A number of methods may be used in order to produce such a calibration. The method demonstrated here is to:

5.1. Find a standard spectrum of a known star
5.2. Observe that star with the current instrument and analysis.
5.3. Find the ratio of the observed spectrum to the standard spectrum
5.4. Use this ratio to correct further observations

Figure 26 shows a standard spectrum of Vega. The data are read from files on an ESO web site.

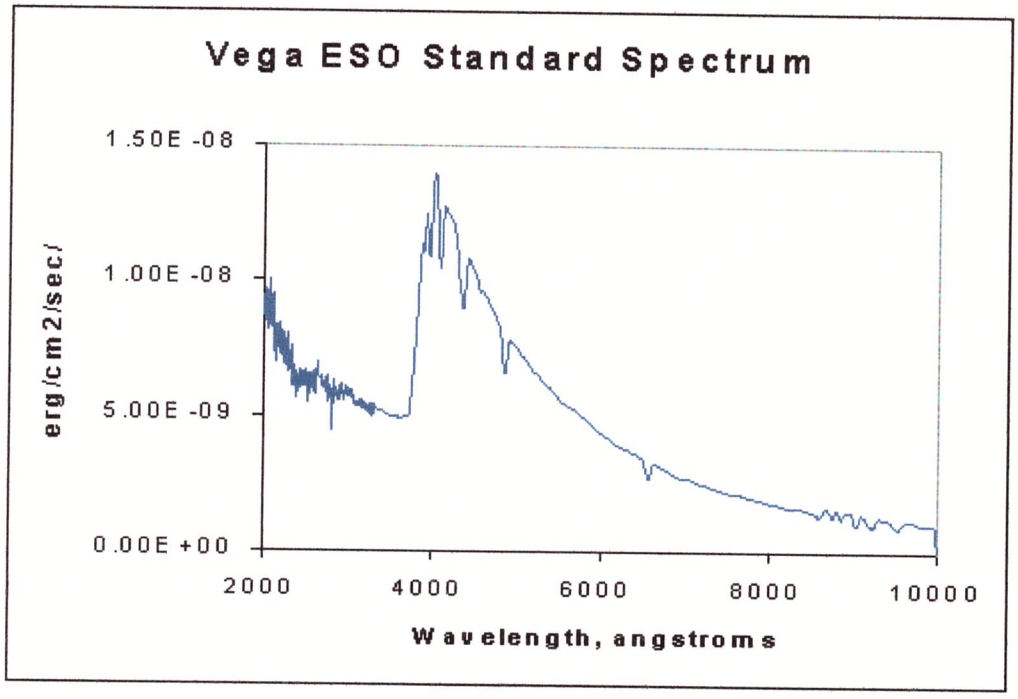

Figure 26. Standard spectrum of Vega.

The ultra violet response is a little strange and needs to be resolved in further work, but the spectrum serves as an example here. Vega was then observed using the 70 line/mm grating and the raw data spectrum shown in Figure 27 was produced.

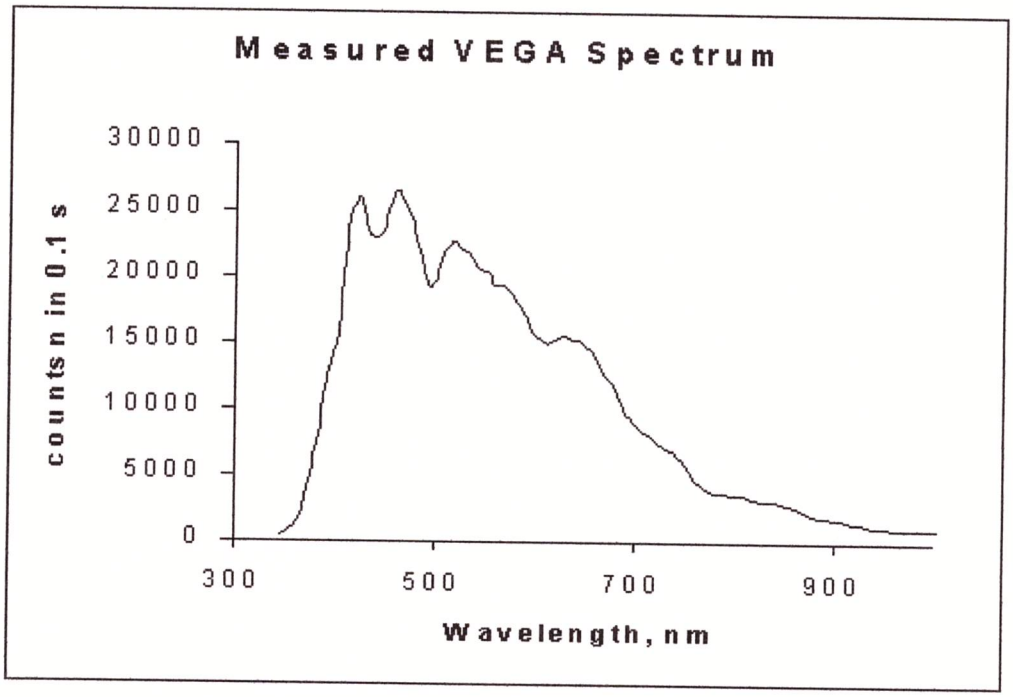

Figure 27. Measured spectrum of Vega.

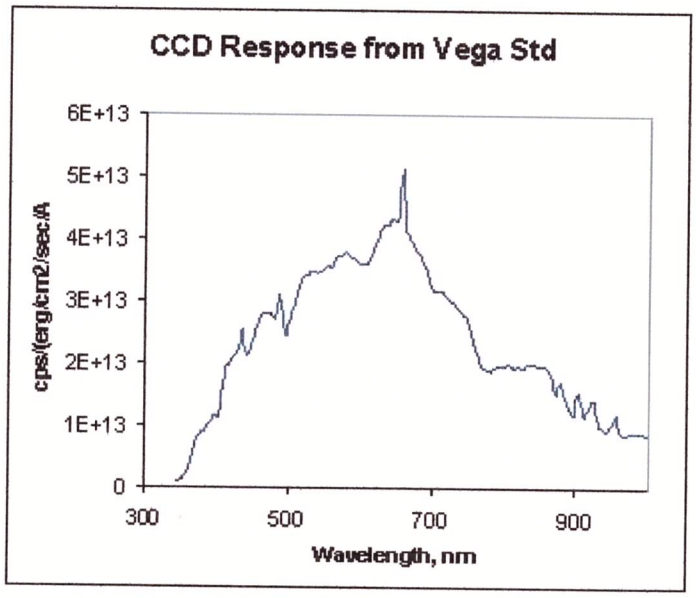

Figure 28. Response of CCD chip measured using Vega spectrum.

The ratio of the measured response, shown in Figure 27, to the standard flux, shown in Figure 26 was formed point by point using interpolation as required. The response,

shown in Figure 28, shows some irregularities which are not expected to be real but which are likely attributable to the differences in resolution in the two spectra. Application of this response function can then be demonstrated by correcting the measured Vega spectrum. The resulting corrected and uncorrected spectra are shown in Figure 29 together.

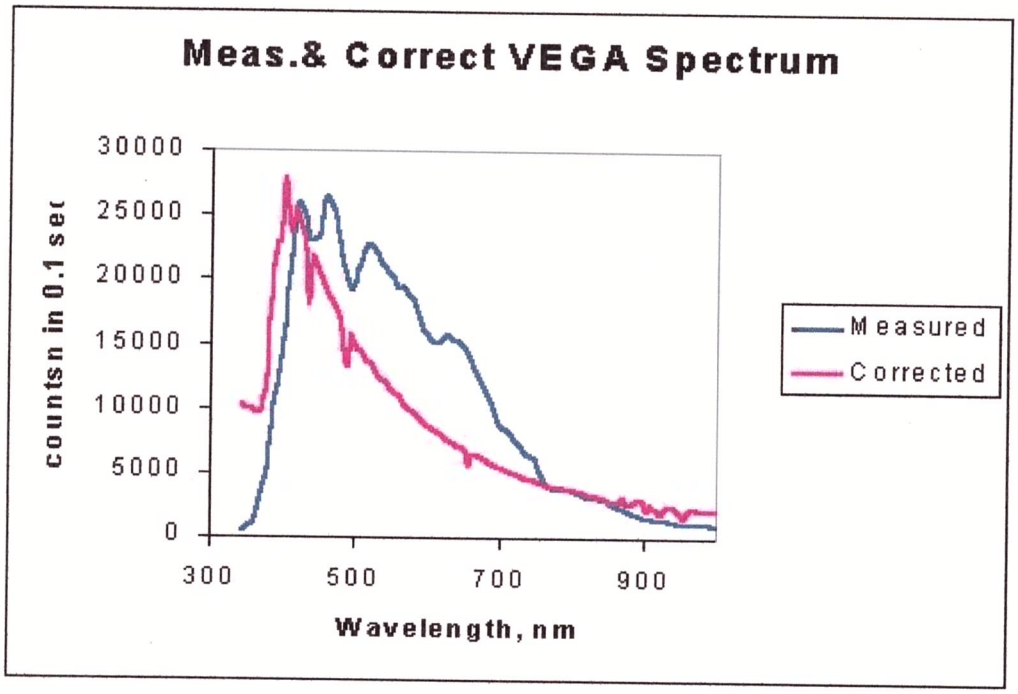

Figure 29. Comparison of measured and response corrected spectra for Vega.

6.0. Conversion to UBVRI. In order to reach the ultimate goal of the project, the tabulated bandpass functions of the standard U, B, V, R, and I filters were coded into the working calculational computer program. Using these functions the values of the bands are readily displayed for any processed image. Figure 30 shows the result of processing 3 asteroid images to product the values of the bandpasses. The asteroids show similar bandpass category values with some possible differences.

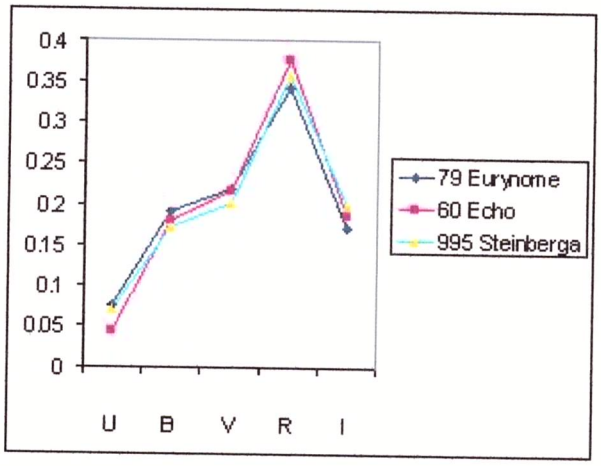

Figure 30. UBVRI values for 3 asteroids determined by the methods developed above.

The category data of Figure 30 will likely represent the end product of a project directed at characterizing the reflectance of the asteroids.

7.0 Statistical Issues. The least detectable object depends on a number of factors:

Darkness of the sky is an important factor. It is optimized by choosing a naturally dark sky site, avoiding bright moon periods, and making repeated measurements which allow rejection of interference by starlight.

Exposure time may be extended almost indefinitely if good tracking is employed. All faint object work should be undertaken with the possibility of up to one hour of data per observation.

The data reduction method must be optimized to provide for local subtraction of background data, eliminating the effects of dark noise and field unflatness for each image.

The bin width in final reporting will reflect the noise in the spectrum. The filter pass bands are not uniform in width and may be the subject of further standardization.

The camera characteristic should be optimized to have pixel size of the order of magnitude of the resolution of the telescope. Over sampling by using too small a bin size is preferred to under sampling by using large bins thereby sacrificing brightness.

Telescope collimation/focus is a critical issue in producing the brightest possible image and great care should be taken to ensure as good quality as can be had.

8.0 Summary. These tests have shown the possibility of routine spectroscopy of asteroids down to magnitude 16 with sufficient resolution to permit the reporting of color categories. The methodology is capable of being made routine for the brighter asteroids

and, with some added care, can be made routine for the fainter ones. The use of the converging beam grating method avoids all critical alignment issues and results in an image that is easy to interpret.